ORIGINAL RESEARCH

Extracellular Vesicles from *Akkermansia muciniphila* Elicit Antitumor Immunity Against Prostate Cancer via Modulation of CD8^{+} T Cells and Macrophages

Zhong-Wei Luo, [iD][1,2] Kun Xia,[1,2]
Yi-Wei Liu, [iD][1,2] Jiang-Hua Liu,[1,2]
Shan-Shan Rao,[2,3] Xiong-Ke Hu,[1,2]
Chun-Yuan Chen,[1,2] Ran Xu, [iD][4]
Zhen-Xing Wang,[1,2] Hui Xie [iD][1,2,5–8]

[1]Department of Orthopedics, Xiangya Hospital, Central South University, Changsha, Hunan, People's Republic of China; [2]Movement System Injury and Repair Research Center, Xiangya Hospital, Central South University, Changsha, Hunan, People's Republic of China; [3]Xiangya Nursing School, Central South University, Changsha, Hunan, People's Republic of China; [4]Department of Urology, The Second Xiangya Hospital, Central South University, Changsha, Hunan, People's Republic of China; [5]Department of Sports Medicine, Xiangya Hospital, Central South University, Changsha, Hunan, People's Republic of China; [6]Hunan Key Laboratory of Organ Injury, Aging and Regenerative Medicine, Changsha, Hunan, People's Republic of China; [7]Hunan Key Laboratory of Bone Joint Degeneration and Injury, Changsha, Hunan, People's Republic of China; [8]National Clinical Research Center for Geriatric Disorders, Xiangya Hospital, Central South University, Changsha, Hunan, People's Republic of China

Correspondence: Hui Xie
Department of Orthopedics, Xiangya Hospital, Central South University, 87 Xiangya Road, Changsha, Hunan, 410008, People's Republic of China
Email huixie@csu.edu.cn

Ran Xu
Department of Urology, The Second Xiangya Hospital, Central South University, 139 Middle Renmin Road, Changsha, Hunan, 410011, People's Republic of China
Email xuran@csu.edu.cn

Purpose: Prostate cancer (PCa) is one of the most common malignancies in males. Despite the success of immunotherapy in many malignant cancers, strategies are still needed to improve therapeutic efficacy in PCa. This study aimed to investigate the effects of *Akkermansia muciniphila*-derived extracellular vesicles (*Akk*-EVs) on PCa and elucidate the underlying immune-related mechanism.

Methods: *Akk*-EVs were isolated by ultracentrifugation and intravenously injected to treat syngeneic PCa-bearing immune-competent mice. Immunophenotypic changes in immune cells, such as cytotoxic T lymphocytes and macrophages, were measured via flow cytometry analysis. Histological examination was used to detect morphological changes in major organs after *Akk*-EVs treatments. In vitro, flow cytometry was performed to confirm the effects of *Akk*-EVs on the activation of CD8^{+} T cells. Quantitative PCR and immunofluorescence staining were carried out to test the impact of *Akk*-EVs on macrophage polarization. Cell counting kit-8 (CCK-8) analysis, colony formation assays, and scratch wound healing assays were conducted to assess the effects of *Akk*-EVs-treated macrophages on the proliferation and invasion of PCa cells. CCK-8 assays also confirmed the impact of *Akk*-EVs on the viability of normal cells.

Results: Intravenous injection of *Akk*-EVs in immune-competent mice reduced the tumor burden of PCa without inducing obvious toxicity in normal tissues. This treatment elevated the proportion of granzyme B-positive (GZMB^{+}) and interferon γ-positive (IFN-γ^{+}) lymphocytes in CD8^{+} T cells and caused macrophage recruitment, with increased tumor-killing M1 macrophages and decreased immunosuppressive M2 macrophages. In vitro, *Akk*-EVs increased the number of GZMB^{+}CD8^{+} and IFN-γ^{+}CD8^{+} T cells and M1-like macrophages. In addition, conditioned medium from *Akk*-EVs-treated macrophages suppressed the proliferation and invasion of prostate cells. Furthermore, the effective dose of *Akk*-EVs was well-tolerated in normal cells.

Conclusion: Our study revealed the promising prospects of *Akk*-EVs as an efficient and biocompatible immunotherapeutic agent for PCa treatment.

Keywords: *Akkermansia muciniphila*, extracellular vesicles, immunotherapy, prostate cancer, cytotoxic T lymphocytes, macrophages

Introduction

Prostate cancer (PCa) is a common malignancy occurring in the prostate epithelium of older men, and its incidence has been gradually increasing worldwide in recent years.[1,2] Current treatment options for PCa include radiation therapy, minimally invasive ablative surgery, androgen deprivation therapy, and radical prostatectomy.[3,4] Although

progression-free survival in low-risk and early-stage patients is favorable, most PCa patients eventually progress to castration-resistant PCa after castration, and the treatment options for this advanced-stage and metastatic disease are limited and not satisfactory.[3,5] Thus, new treatments and therapeutic advances are still urgently needed.

In recent years, cancer immunotherapy has been regarded as one of the most promising strategies for tumor treatment due to its ability to boost the immune system, potential efficiency in various cancers, and feasible long-lasting effects.[6] Numerous ongoing cancer investigations are now focusing on tumor immunotherapy, including nonspecific immune stimulation, immune checkpoint blocking, adoptive cell transplantation, and vaccination strategies.[7,8] These therapeutic strategies have led to many breakthroughs in cancer research, regulating antitumor immunity and bringing survival benefits to many cancer patients.[9] However, different tumor immunotherapy regimens present various effects in PCa patients.[3,10] For instance, the therapeutic vaccine sipuleucel-T has shown a survival benefit in PCa patients, while clinical trials using immune blockade agents, such as ipilimumab, have failed to present impressive outcomes.[3,11,12] Hence, it is essential to develop more efficient strategies to potentiate the efficacy of immunotherapy in the PCa tumor environment.

One of the approaches is integrating nanomedicine with cancer immunotherapy to improve clinical responses while mitigating possible side effects.[13,14] Biogenic nano-sized extracellular vesicles (EVs), secreted by both eukaryotic and prokaryotic cells, are enriched in molecules from host cells, including nucleic acids, proteins, lipids, and lipopolysaccharides.[15] Recently, abundant studies have shown that EVs can be widely used as functional mediators for parent cells or modified for desired purposes, such as modulating antitumor responses.[16,17] *Akkermansia muciniphila* (*Akk*) is a Gram-negative anaerobic bacterium that contributes to homeostasis maintenance and barrier integrity in the gastrointestinal tract.[18,19] Recently, it was reported that supplementation with *Akk* promotes the immunotherapy efficacy in a mouse melanoma tumor model via the modulation of immunological responses by increasing the $CCR9^+CXCR3^+CD4^+$ T lymphocyte infiltration.[20] Although this study elucidated the cause-effect relationship between the clinical response to programmed cell death protein 1 (PD-1) blockade and the distinct commensal abundance of *Akk*, the immunomodulatory effects of *Akk* in cancer remain largely unexplored.

However, to date, the roles of EVs derived from *Akk* (*Akk*-EVs) in PCa tumor immunity have not been described.

In the present study, we isolated and purified EVs from *Akk* and investigated their therapeutic effects in an immune-competent PCa-bearing mouse model. Moreover, we described the immunologic changes mediated by *Akk*-EVs and evaluated these effects in vitro. Our investigation provides a new strategy for developing an effective *Akk*-EVs-based cancer vaccine or adjuvant immunotherapy in the future.

Materials and Methods
Culture of *Akk*
Akk (ATCC, BAA-835, Manassas, USA) was cultured in brain-heart-infusion broth (BD Bioscience, San Jose, USA) containing 0.5% porcine mucin (Sigma-Aldrich, Saint Louis, USA) and 0.05% L-cysteine (Sigma-Aldrich) under anaerobic conditions. The bacteria were shaken constantly and cultured at 37 °C, as previously described.[21] The concentration of bacteria was detected by measuring optical density (OD) at 600 nm wavelength.

Isolation of *Akk*-EVs
Akk-EVs were obtained by the ultracentrifugation method according to the reported literature.[22] Briefly, the culture medium of *Akk* was harvested by centrifugation twice at $6,000 \times g$ for 30 min at 4 °C and then filtered through a 0.45 μm filter (Millipore, Billerica, USA). The medium was then concentrated with Amicon Ultra-15 Centrifugal Filter (100 kDa; Millipore), and the EV pellet was obtained by serial gradient centrifugation with OptiPrep™ solution (60% w/v iodixanol; Sigma-Aldrich) at $100,000 \times g$ for 18 h at 4 °C.[23] Collected EVs were resuspended in PBS and filtered through a 0.22 μm filter to avoid any contamination. After total protein concentration quantification, EVs were stored at −80 °C for further study.

Animals and Treatments
Animal protocols and experimental procedures were approved by the Ethical Committee at Xiangya Hospital, Central South University, and performed in accordance with the Guidelines for the Care and Use of Laboratory Animals of the Ethical Committee at Xiangya Hospital. To investigate the effects of *Akk*-EVs on tumor immunity, we used C57BL/6 male mice (8 weeks old) with an intact immune system in the present study. The RM-1 (a mouse PCa cell line derived from the C57BL/6 strain) was subcutaneously inoculated (1×10^6 cells per mouse) into the

mice's right axilla to establish the syngeneic tumor mouse model. Five days after RM-1 inoculation, these mice were randomly divided into two groups (n = 5 per group), which were respectively injected with solvent (normal saline) or *Akk*-EVs (40 μg per mouse) every other day through the tail vein. The tumor length and width were measured three times a week using a vernier caliper. The tumor volume (V) was calculated by the formula: V = (length × width^2)/ 2. Body mass, as well as food and water consumption, were recorded during the experiments. The mice were sacrificed after 13 days of treatment. Blood cells were collected for flow cytometry analysis, and subcutaneous tumors were excised and weighed for further analysis. The major organs, including the liver and kidney, were also harvested for systemic toxicity analysis.

Flow Cytometry

For flow cytometry analysis of the mice specimen, single-cell suspensions were first prepared. Tumor tissue was gently ground and filtered through a 70 μm nylon mesh strainer. Collected blood was mixed with red blood cell lysis buffer (Solarbio, Beijing, China) to remove the erythrocytes. The cells were resuspended and counted for the next steps. Cells were generally stained with Zombie Aqua™ Fixable Viability Kit (423102; Biolegend, San Diego, USA) or Fixable Viability Stain 620 (FVS620, 564996; BD) to distinguish live/dead cells. After blocking the IgG Fc portion with CD16/CD32 (101320; Biolegend) antibody, cells were divided into several tubes and stained in different antibody panel containing varied cell-surface markers, including APCCY7-CD45 (557659; BD), PECY7-CD8α (552877; BD), FITC-CD11b (101206; Biolegend), PE-F4/80 (123110; Biolegend), and BV421-MHC-II (107632; Biolegend) in recommended concentrations at 4 °C for 30 min. After fixation and permeabilization by Cytofix/Cytoperm Plus kit (BD), intracellular granzyme B (GZMB), CD206, and interferon γ (IFN-γ) were stained using APC-GZMB (17-8898-82; ThermoFisher, Waltham, USA), APC-CD206 (141708; Biolegend), and BV421-IFN-γ (563376; BD) antibodies. For the T cell intracellular IFN-γ cytokine staining, cells were stimulated with 50 ng/mL phorbol 12-myristate 13-acetate (PMA; Sigma-Aldrich), 1 μg/mL ionomycin (Tocris, Bristol, UK), and 5 μg/mL protein transport inhibitor (BD) for 6 h after cell counting. Fluorescence Minus One (FMO) control was used for gating analysis. For flow cytometry analysis of cultured cells, cells were washed and centrifuged. After being

resuspended and counted, cells were stained with FVS620, CD8α, GZMB, and IFN-γ as described above. Data of stained cells were acquired by FACS DXP Athena (Cytek, Fremont, USA) flow cytometer with Flowjo CE software. Data were further analyzed by FlowJo software version 10.0.

Histological and Immunofluorescence Staining Analysis

Tumor and organ tissues were fixed, dehydrated, and embedded in paraffin. Then the tissue paraffin blocks were cut into 5-μm-thick slices. After being deparaffinized, rehydrated, slices were subjected to histological and immunofluorescence staining. For histological examination, sections of organ tissues were performed with hematoxylin and eosin (H&E) staining according to the instruction (Servicebio, Wuhan, China). Immunofluorescence staining of Ki67, a cell proliferation marker, was performed as previously described.[24] Briefly, sections were performed with antigen retrieval in 10×10^{-3} M citrate buffer (pH 6.0) at 95 °C and blocked with 3% bovine serum albumin. The sections were then incubated with the primary antibody anti-Ki67 (1:200; GB13030–2; Servicebio) at 4 °C overnight. Following washing, they were incubated with secondary antibody (1:200; 711-295-152; Jackson ImmunoResearch, West Grove, USA). Nuclei were counterstained and mounted with the antifade mounting medium with DAPI (H-1200; Vector Laboratories, Burlingame, USA). For CD86 staining, cells were seeded in climbing slices. The treated cells were fixed in 4% paraformaldehyde and then permeabilized with 0.25% TritonX-100/PBS. After blockage with 5% goat serum/0.25% Triton/PBS, cells were then incubated with the primary antibody anti-CD86 (1:200; NBP2–25208; Novus Biologicals, Littleton, USA) and secondary antibody (1:300; 115-545-003; Jackson ImmunoResearch). The nuclei were stained by DAPI. Images were captured with a Zeiss fluorescence microscope equipped with an ApoTome.2 system or Olympus CX31 microscope. For Ki67-positive cell counting, three slides per group were calculated.

Cell Culture

Mouse PCa cell line RM-1 and human PCa cell line DU-145 and PC-3 were purchased from Zhong Qiao Xin Zhou Biotechnology Company (Shanghai, China).

Human monocytic leukemia cell line THP-1 and mouse leukemic macrophages cell line RAW264.7 were purchased from Procell Life Science Technology Company (Wuhan, China). Human VSMC (vascular smooth muscle cell) was purchased from Fu Heng Biology Co. (Shanghai, China), and HMEC (human microvascular endothelial cells) were purchased from Cell Bank of the Chinese Academy of Sciences (Shanghai, China). Human prostate hyperplasia cell line BPH-1 was kindly gifted from Prof. Long Wang (The Third Xiangya Hospital, Changsha, China), and the use of the gifted cell line has been approved by the Ethical Committee at Xiangya Hospital. RM-1 and BPH-1 were cultured in RPMI 1640 medium (Biological Industries, Beit HaEmek, Israel) supplemented with 10% fetal bovine serum (FBS; Gibco, Grand Island, USA) and 1% Penicillin/Streptomycin (P/S, 100 U/mL; Solarbio). DU-145 and RAW264.7 were cultured in DMEM (Gibco) medium with 10% FBS and 1% P/S. PC-3 was cultured in DMEM/F-12 (Gibco) with 10% FBS and 1% P/S. THP-1 cells were cultured in RPMI-1640 medium with 10% FBS, 1% PS, and 0.05 mM β-mercaptoethanol. VSMC was cultured in F12K medium (Hyclone, Logan, USA) with 10% FBS and 1% P/S. HMEC was cultured in MCDB131 medium (Gibco) with 10% FBS and 1% GlutaMAX (Gibco). All cells were maintained at 37 °C in a humidified atmosphere with 5% CO_2.

For mouse naïve $CD8^+$ T Cell isolation, the commercial isolation kit (480008; Biolegend) was used according to the manufacturer's protocol. Briefly, the spleens of C57BL/6 mice were harvested and softly ground for single-cell suspension. Single cells were incubated with the biotin antibody cocktail followed by incubation with magnetic streptavidin nanobeads. Non-$CD8^+$ T cells were depleted using a magnetic separator. $CD8^+$ T cells were cultured in RPMI-1640 medium with 10% FBS and 1% PS in the presence of 1 mM pyruvic acid sodium, 0.05 mM β-mercaptoethanol, and 10 ng/mL of IL-2 (51061-MNAE; Sino Biological, Beijing, China) for two days. Anti-mouse CD3ε/CD28 antibodies (2 μg/mL; 100339 and 102115, Biolegend) were also used to stimulate T cells' proliferation.

Preparation of Condition Medium (CM) from Akk-EVs-Treated Macrophages

THP-1 cells were treated with 100 ng/mL PMA for 48 h to obtain PMA-differentiated THP-1 macrophages followed by one day in the complete medium without PMA. Subsequently, differentiated THP-1 or RAW264.7 macrophages were incubated with *Akk*-EVs (10 μg/mL) or an equal volume of solvent (PBS) for 24 h. The CM of *Akk*-EVs-treated (CM $^{(Akk\text{-}EVs)}$) or solvent-treated (CM $^{(solvent)}$) macrophages were collected and centrifuged at 2000 × g for 10 min to remove dead cells and cellular debris. The supernatant was filtered through 0.22 μm filters and stored at −80 °C for downstream experiments.

Cell Counting Kit-8 (CCK-8) Assay

Cell viability was assessed by CCK-8 assay as previously described.[25] Briefly, cells (5×10^3 cells per well) were seeded into 96-well culture plates and incubated for 24 h. Next, the medium was replaced with complete medium supplemented with different treatment agents, and the cells were incubated for another 24 h. After that, cells were then incubated for 3 h in 100 μL fresh medium with 10 μL CCK-8 reagent (7Sea Biotech, Shanghai, China), and OD values were measured using a microplate reader (Varioskan LUX, Thermo Scientific, Waltham, USA) at 450 nm wavelength. A group without cells served as the blank. The viability of cells (%) of the control group (CM $^{(solvent)}$-treated or solvent-treated) was set as 100%, and that of other experimental groups (CM $^{(Akk\text{-}EVs)}$-treated or *Akk*-EVs-treated) was calculated by the following formula: viability (%) = (mean OD of cells of the experimental group − mean OD of blank)/(mean OD of cells of the control group − mean OD of blank) × 100.

Colony Formation Assay

Cells (0.2×10^3 cells per well) were seeded into 6-well culture plates and treated with the above-described CM for 14 days. Then cells were stained with 0.5% crystal violet (Solarbio) for 5min, and the numbers of colonies (> 50 cells per colony) were photographed and manually quantified.

Scratch Wound Healing Assay

Cells (2×10^5 cells per well) were seeded into 12-well culture plates and treated with the above-described CM. Once the cells were approximately 100% confluent, the monolayer was scratched using a sterile p200 pipette tip. Unattached cells were removed by gentle washing. Then, the attached cells were treated with the above-collected CM. Mitomycin-C (5 μg/mL; Sigma-Aldrich) was also added to avoid the effects of cell proliferation on wound closure. Images of different cells were photographed at various time points under an inverted microscope (AE2000, Motic,

China). The following formula calculated the ratio of migration area: migration area (%) = (A0 − Ar)/A0 × 100, where A0 represents the area of the initial wound area, Ar represents the remaining wound area at indicated time point.

Quantitative Real-Time PCR Analysis

Total RNA was extracted from the treated THP-1 cells using TRIzol reagent (Takara Biotechnology, Japan) and reverse-transcribed into cDNA by All-in-One cDNA Synthesis SuperMix (Bimake, Houston, USA) according to the manufacture's protocol. The cDNA was amplified using 2× SYBR Green qRT-PCR Master Mix (Bimake) on an FTC-3000 real-time PCR system (Funglyn Biotech Inc., Toronto, Canada). The PCR results were analyzed using the $2^{-\Delta\Delta CT}$ method.[26] GAPDH was selected as the internal reference. All primers were synthesized by Sangon Biotech Co., Ltd (Shanghai, China). The primer sequences for human used in this study were as follows: *INOS*: forward, 5′-TTCAGTATCACAACCTCAGCAAG -3′, and reverse, 5′-TGGACCTGCAAGTTAAAATCCC -3′; *CD68*: forward, 5′-CTTCTCTCATTCCCCTATGGA CA-3′, and reverse, 5′-GAAGGACACATTGTACTCCA CC-3′; *IL-1β*: forward, 5′-CCACAGACCTTC CAGGAGAATG-3′, and reverse, 5′-GTGCAGTT CAGTGATCGTACAGG-3′; *GAPDH*: forward, 5′- GGAGCGAGATCCCTCCAAAAT-3′, and reverse, 5′- GGCTGTTGTCATACTTCTCATGG-3′.

Statistical Analysis

All descriptive statistical data were presented as mean ± standard error of mean (SEM). Two-group comparisons were analyzed by unpaired, two-tailed Student's *t*-test. Statistical analyses were conducted using GraphPad Prism 7 software. A value of $P < 0.05$ was considered to indicate a statistically significant difference. * $P < 0.05$, ** $P < 0.01$, *** $P < 0.001$, **** $P < 0.0001$.

Results

Characterization of *Akk*-EVs

First, we isolated EVs from the culture medium of *Akk* and then characterized the isolated EVs using transmission electron microscopy (TEM) and dynamic light scattering (DLS) analysis. As shown in Figure 1A and B, *Akk*-EVs exhibited typical cup-shaped or spherical morphologies with a diameter of 181.9 ± 42.4 nm, similar to previously described EVs derived from bacteria.[27,28] These data indicate that *Akk*-EVs were successfully collected.
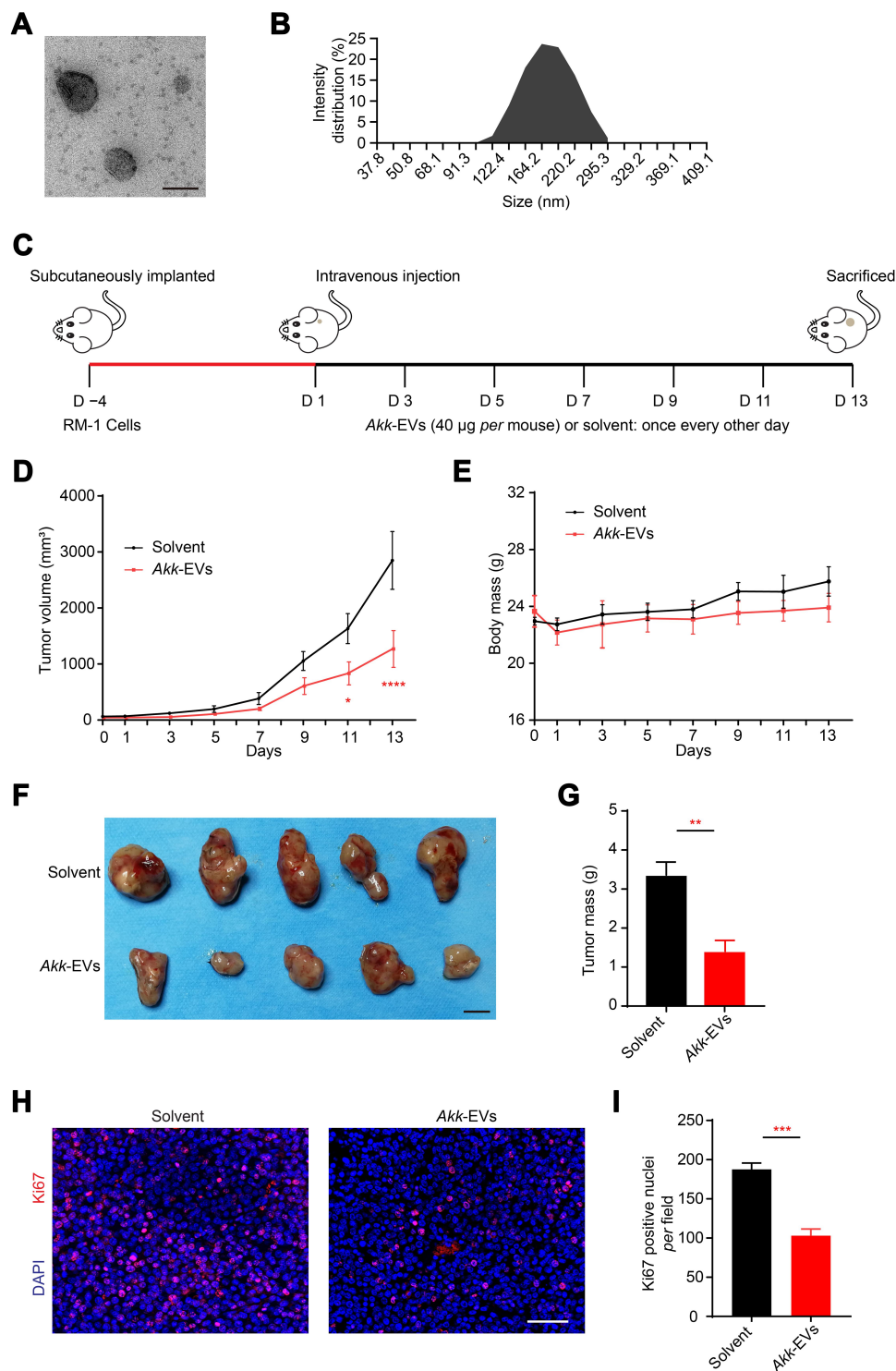
Akk-EVs Reduced Tumor Burden in a PCa Mouse Model

To explore the in vivo effects of *Akk*-EVs on PCa growth, we constructed syngeneic tumor models via subcutaneous inoculation of RM-1 cells in immune-competent C57BL/6 mice. Mice with an intact immune system elicit a robust immune response to tumors and reflect the efficacy of *Akk*-EVs on the immune system.

A schematic diagram is illustrated in Figure 1C. In *Akk*-EVs-treated mice, tumor growth progression was significantly slowed compared with solvent-treated control mice (Day 11: $P = 0.0272$, Day 13: $P < 0.0001$; Figure 1D). In general, no significant difference in the average body mass was observed between the two groups, and the body mass of both groups gradually increased during the later observation period (Figure 1E), suggesting that these tumor-bearing mice did not develop cancer cachexia. The weight difference between the two groups might result from the slower tumor growth in *Akk*-EVs-treated mice. At the end of the intervention, the size of tumor specimens from mice with *Akk*-EVs treatment was smaller than that from solvent-treated control mice (Figure 1F). *Akk*-EVs induced nearly 60% inhibition of tumor growth on day 13 ($P = 0.0019$; Figure 1G). Cell proliferation was assessed by immunofluorescence staining of Ki67. As evidenced in Figure 1H, systemic administration of *Akk*-EVs significantly reduced the number of proliferating cells within the tumors. The counts of Ki67-positive cells also confirmed this observation ($P = 0.0002$; Figure 1I). Taken together, these findings demonstrate the potent antitumor efficacy of *Akk*-EVs against PCa due to their powerful function in inhibiting proliferation.

Akk-EVs Elevated the Proportion of GZMB⁺ and IFN-γ⁺ Lymphocytes in CD8⁺ T cells in vivo and in vitro

To evaluate the effects of *Akk*-EVs related to the antitumor immune response, we first assessed CD8⁺ cytotoxic T lymphocytes (CTLs) in vivo. Using flow cytometry, we found that the activity of GZMB and IFN-γ in infiltrated CD8⁺ T cells was significantly enhanced in tumors from *Akk*-EVs-treated groups, as shown in representative plots (Figure 2A and C) and quantification analysis ($P = 0.0309$; Figure 2B and $P = 0.0492$; Figure 2D). Similarly, in the peripheral blood (Figure S1A-D), we observed a significantly higher proportion of GZMB⁺CD8⁺ T cells in the *Akk*-EVs-treated group (P = 0.0040; Figure S1B), and IFN-γ⁺CD8⁺ T cells showed the same trend, although

Figure 1 *Akk*-EVs reduced tumor burden in a PCa mouse model. (**A**) Representative TEM image of *Akk*-EVs. Scale bar: 200 nm. (**B**) The particle size distribution of *Akk*-EVs detected by DLS. (**C**) Schematic diagram of the treatment schedule for subcutaneous RM-1 tumor-bearing C57BL/6 mice. (**D**) Tumor volumes of mice in different treatment groups are shown at the indicated times during the observation period of 13 days. n = 5 per group. (**E**) Body mass of mice were recorded during the whole experiment. n = 5 per group. (**F** and **G**) Digital photographs (**F**) and the mass (**G**) of tumor tissues isolated from the RM-1 tumor-bearing mice on the 13th day after different treatments. Scale bar: 1 cm. n = 5 per group. (**H** and **I**) Representative images (**H**) and quantification (**I**) of Ki67 immunofluorescence staining of tumor sections. Scale bar: 50 μm. n = 3 per group. Data are shown as mean ± SEM. *$P < 0.05$, **$P < 0.01$, ***$P < 0.001$, ****$P < 0.0001$.

the difference was not statistically significant (P = 0.0642; Figure S1D).

Next, we examined the effects of *Akk*-EVs on GZMB and IFN-γ expression in CD8$^+$ T cells in vitro. *Akk*-EVs treatment significantly increased the proportion of GZMB$^+$ cells in CD8$^+$ T cells compared to the solvent treatment group (representative image in Figure 2E and statistical analysis in Figure 2F: P = 0.0179). Likewise, the *Akk*-EVs-treated group exhibited a drastically higher proportion of IFN-γ$^+$CD8$^+$ T cells than the control group (representative image in Figure 2G and statistical analysis in Figure 2H: P = 0.0367). These results suggest that the *Akk*-EVs treatment provoked a CTL-mediated antitumor response.

Akk-EVs Recruited Macrophages and Skewed Them to an M1-Like Phenotype

We also examined the macrophages in the tumor microenvironment (TME) of RM-1 tumors using flow cytometry analysis. We observed a significantly increased proportion of F4/80$^+$ macrophages to total CD11b$^+$ myeloid cells in the *Akk*-EVs-treated group compared to the solvent-treated group (representative image in Figure 3A and statistical analysis in Figure 3B: P = 0.0181). While macrophages are recognized to exhibit a complex spectrum of activation status, we further analyzed the expression of MHC-II and CD206 (M1 and M2 macrophage markers, respectively) to define the activation states of macrophages within the TME.[29] A higher proportion of M2 macrophages is associated with a poorer prognosis, while the M1 population can enhance tumor-killing effects.[30,31] We observed a significant increase in M1 macrophages in the tumors from *Akk*-EVs-treated mice (representative image in Figure 3C and statistical analysis in Figure 3D: P = 0.0155), as well as a decrease in M2 macrophages (P = 0.0318; Figure 3E), while the proportion of an intermediate state of macrophages (expressing both MHC-II and CD206) remained unchanged (P = 0.4425; Figure 3F). We also examined the populations of macrophages in the peripheral blood. Flow cytometry analysis results showed a similar trend as in the tumor, although the difference was not statistically significant (P = 0.2061, 0.2312, 0.3687, 0.3549 respectively in Figure S2A-D).

We further tested whether *Akk*-EVs affected macrophage polarization in vitro. PMA-stimulated THP-1 cells were treated with solvent or 10 ng/μL *Akk*-EVs. After *Akk*-EVs treatment, the differentiated THP-1 macrophages exhibited an irregular morphology with longer cellular pseudopodia

compared to the control group (Figure S2E), indicating changes in the differentiation of these cells. Immunofluorescence staining confirmed that *Akk*-EVs upregulated the expression of CD86 in macrophages (representative image in Figure 3G and statistical analysis in Figure 3H: P = 0.0033). According to the qPCR results, the mRNA expression levels of *INOS, IL-1β*, and *CD68* (characterized as M1 macrophages[32]) in *Akk*-EVs-treated cells were significantly increased than those in the control group (*INOS:* P = 0.0060, *IL-1β:* P = 0.0465, *CD68:* P = 0.0066; Figure 3I). RAW264.7 mouse macrophage-like cells were also treated with *Akk*-EVs. Immunofluorescence staining results (Figure S2F) showed that the intensity of CD86$^+$ cells was increased after *Akk*-EVs treatment (P = 0.0007; Figure S2G), which was consistent with the observation in THP-1 cells. These data suggest that *Akk*-EVs modified macrophage polarization, predominantly toward an M1-like phenotype, contributing to the antitumor response in the TME.
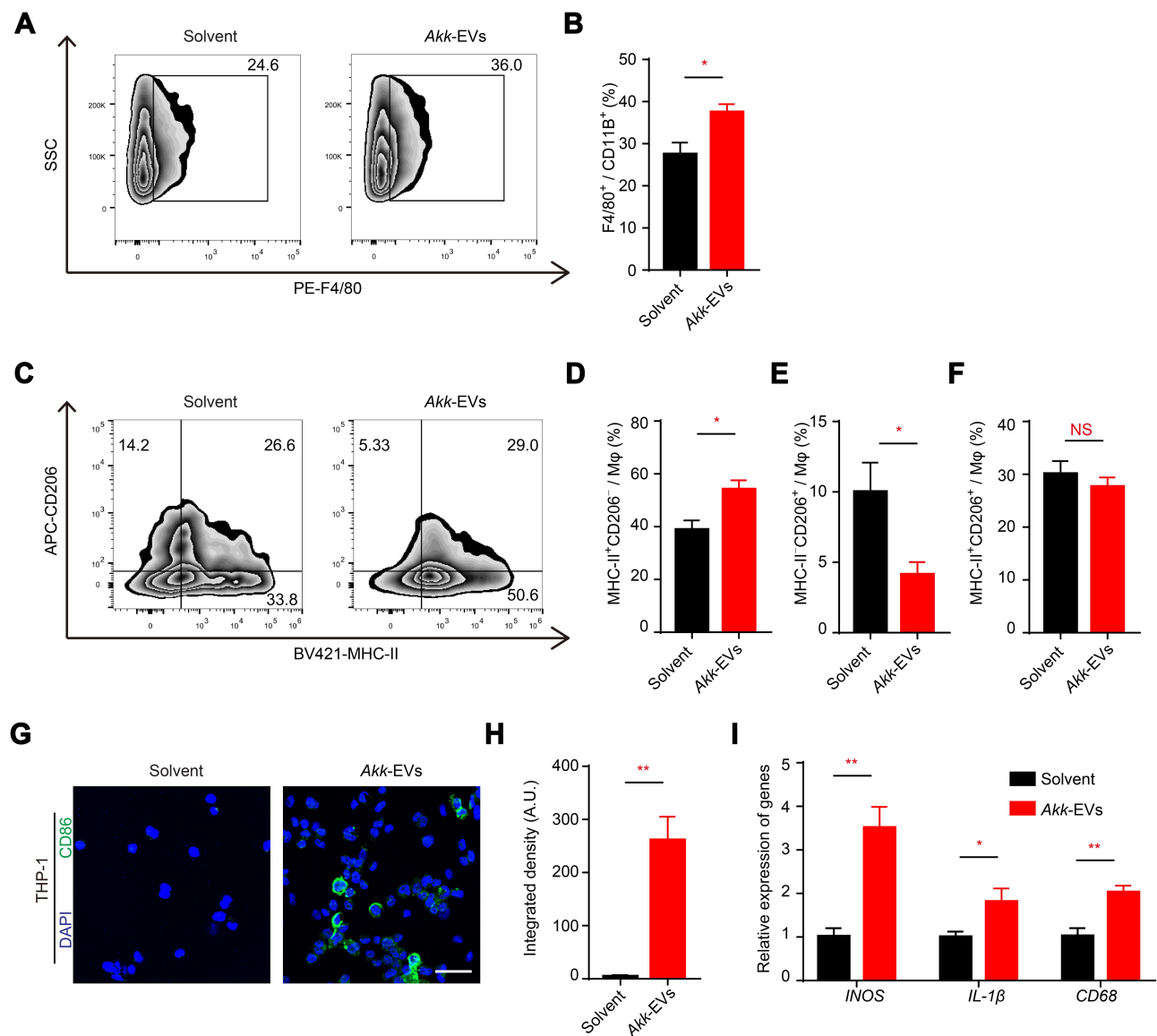
Akk-EVs-Treated Macrophages Suppressed the Proliferation and Invasion of PCa Cells

To explore the impact of *Akk*-EVs-treated macrophages on tumor cells, we collected the CM of PMA-stimulated THP-1 cells in the presence of *Akk*-EVs or solvent. CCK-8 assays were used to test the effects of the CM on the viability of human PCa cell lines. Compared to CM $^{(solvent)}$ treatment, incubation with CM $^{(Akk-EVs)}$ for 24 h decreased the proliferation of DU145 cells (P = 0.0043; Figure 4A) and PC-3 cells (P = 0.0371; Figure 4C). We then assayed the influence of CM $^{(Akk-EVs)}$ on the colony formation capacity of DU145 and PC-3 cells. CM $^{(Akk-EVs)}$ coculture significantly weakened the ability to form colonies, suggesting the inhibition on the malignancy of cancer cells (P = 0.0369; Figure 4B and P = 0.0216; Figure 4D).[33] Furthermore, we determined that macrophages pretreated with *Akk*-EVs showed inhibitory effects on the invasion of DU145 and PC-3 cells, evidenced by attenuated wound closure rates in the scratch wound healing assay (representative image in Figure 4E and G, statistical analysis: P = 0.0081, <0.0001 in Figure 3F and P = 0.0049, <0.0001 in Figure 4H).

Consistent with these results in human cell lines, RM-1 mouse PCa cells incubated with CM from *Akk*-EVs-treated RAW264.7 cells presented similar inhibition on cancer cell viability, colony formation, and invasion (P = 0.0324, 0.0018, 0.0017, respectively in Figure S3A-D). Taken
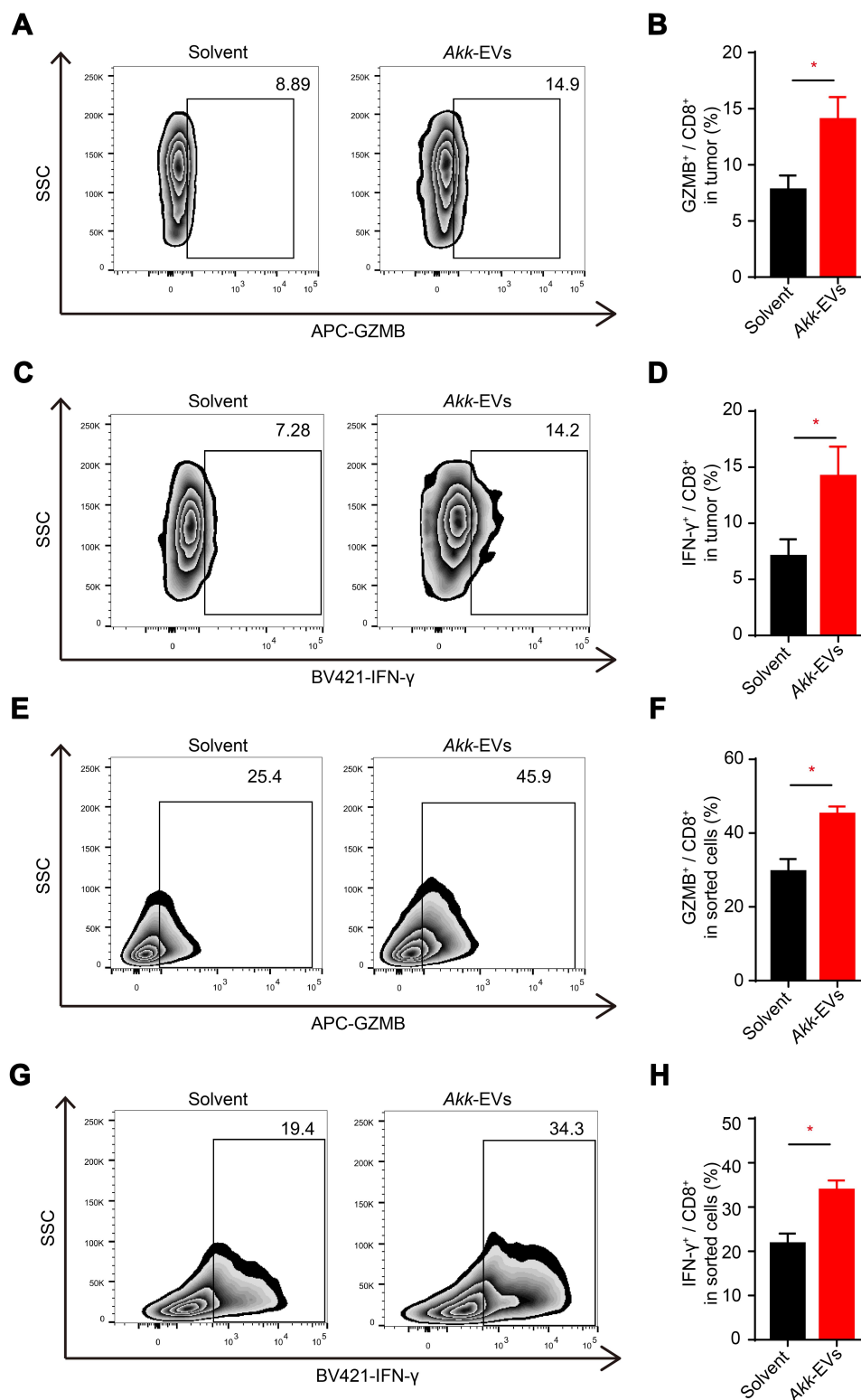
Figure 2 *Akk*-EVs elevated the proportion of GZMB+ and IFN-γ+ lymphocytes in CD8+ T cells in vivo and in vitro. (**A–D**) Flow cytometry analysis of the number of GZMB and IFN-γ of CD8+ T cells infiltrated in PCa tumor tissues of solvent or *Akk*-EVs-treated mice. Representative plots (**A** and **C**) and quantitative analysis (**B** and **D**) were shown. n = 5 per group. (**E–H**) Flow cytometry analysis of GZMB and IFN-γ expression of CD8+ T cells in vitro. Representative plots (**E** and **G**) and quantitative analysis (**F** and **H**). n = 5 per group. Data are shown as mean ± SEM. *P < 0.05.

Figure 3 *Akk*-EVs recruited macrophages and skewed them to an M1-like phenotype. (**A–F**) Flow cytometry analysis of tumor infiltrated macrophages of solvent- or *Akk*-EVs-treated mice. Macrophages (Mφ) were identified as CD11b⁺F4/80⁺ cells. Representative plots (**A**) and quantitative analysis (**B**) of the proportion of F4/80⁺ cells in CD11b⁺ cells were shown. M1-like and M2-like Mφ were identified as MHC-II⁺CD206⁻ and MHC-II⁻CD206⁺, respectively. Representative plots (**C**) showed the gating strategy to define different Mφ phenotypes, and quantitative analysis of different subpopulations was also shown (**D–F**). n = 5 per group. (**G** and **H**) Representative images (**G**) and quantification (**H**) of CD86-stained PMA-pretreated THP-1 after solvent or *Akk*-EVs treatment for 48h. Scale bar: 50 μm. (**I**) qRT-PCR analysis of the expression levels of *INOS, CD68,* and *IL-1β* in PMA-pretreated human THP-1 cells receiving different treatments for 24 h. n = 3 per group. Data are shown as mean ± SEM. *$P < 0.05$, **$P < 0.01$. NS, not significant.

together, these data demonstrate that after *Akk*-EVs treatment, macrophages significantly attenuated cell proliferation and invasion.
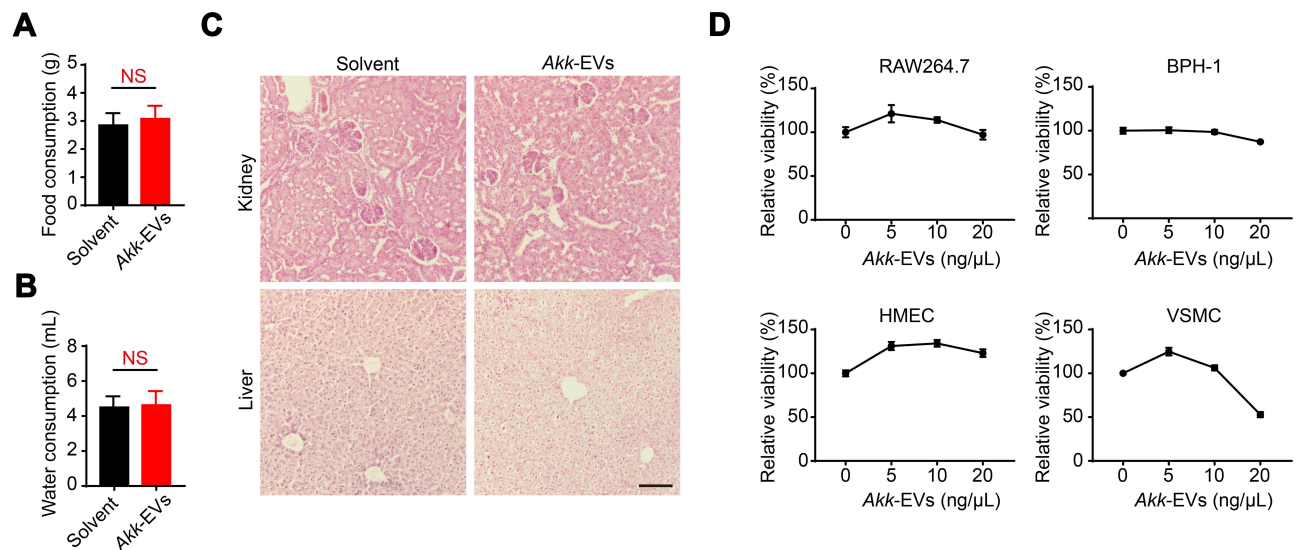
Akk-EVs Were Tolerated in vivo and in vitro

RM-1 tumor-bearing mice treated with *Akk*-EVs exhibited no significant decrease in food intake and water consumption compared with the solvent-treated mice ($P = 0.7113$, 0.9009, respectively in Figure 5A and B), suggesting that

Akk-EVs did not influence the general health condition of the treated mice. Histological analyses based on H&E staining were also performed to assess the toxicity of *Akk*-EVs to critical organs, such as the kidney and liver, in RM-1 tumor-bearing mice. No obvious necrosis or inflammatory infiltration was observed in these organs, indicating that little toxic response occurred in these tissues (Figure 5C). Moreover, the effective dose of *Akk*-EVs did not show remarkable toxic effects on many normal cell lines, including RAW264.7 macrophages, BPH-1
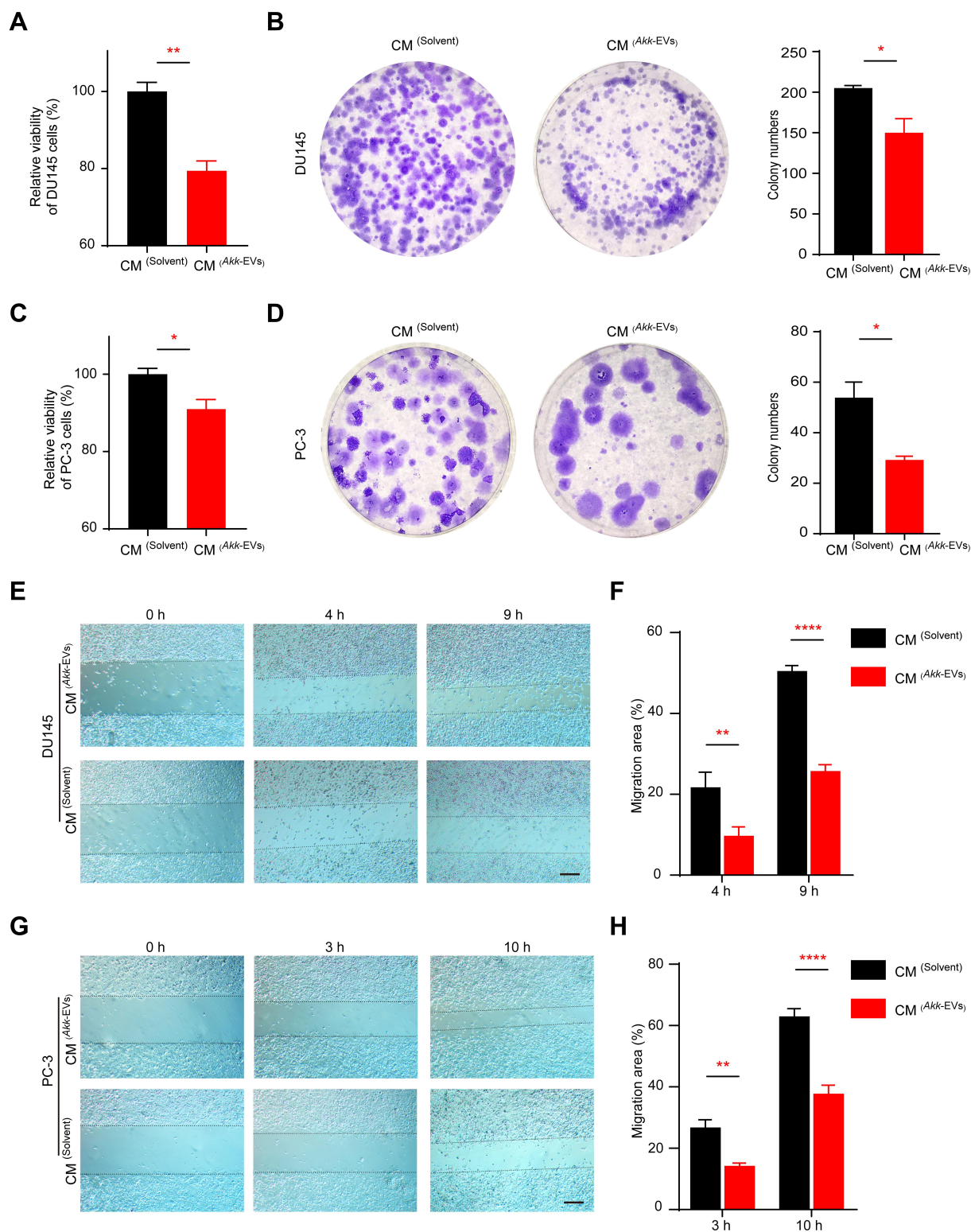
Figure 4 *Akk*-EVs-treated macrophages suppressed the proliferation and invasion of prostate cells. (**A** and **C**) CCK-8 analysis of the viability of human PCa cell line DU145 (**A**) and PC-3 (**C**) cells receiving different CM treatments for 24 h. n = 4 per group. (**B** and **D**) Representative images and quantitative analysis of the crystal violet-stained colonies formed by DU145 (**B**) and PC-3 (**D**) cells receiving different treatments for 14 days. n = 3 per group. (**E**–**H**) Representative images of scratch wound healing assay in DU145 (**E**) and PC-3 (**G**) cells after different CM treatments at indicated time points and corresponding quantification of the migration rates in DU145 (**F**) and PC-3 (**H**). Scale bar: 200 μm. n = 4 per group. Data are shown as mean ± SEM. *P < 0.05, **P < 0.01, ****P < 0.0001.

Figure 5 *Akk*-EVs were tolerated in vivo and in vitro. (**A** and **B**) Average daily food (**A**) and water (**B**) consumption of mice were shown. n = 5 per group. (**C**) Representative H&E staining images of kidney and liver from subcutaneous RM-1 bearing mice treated with solvent or *Akk*-EVs for 13 days. Scale bar: 100 μm. n = 3 per group. (**D**) CCK-8 analysis of the viability of a panel of normal cell lines (RAW264.7, BPH-1, HMECs, and VSMC) receiving different doses of *Akk*-EVs for 24 h. n = 4 per group. Data are shown as mean ± SEM. NS, not significant.

prostate hyperplasia cells, or vascular-related cells, such as HMECs and VSMCs (Figure 5D). Interestingly, it seems that *Akk*-EVs can stimulate proliferation at low concentrations. The results of this short-term study suggest that *Akk*-EVs are well tolerated as a safe agent for cancer therapy.

Discussion

In this study, we demonstrated that intravenous administration of *Akk*-EVs reduced the tumor burden in a PCa-bearing mouse model with an intact immune system. Furthermore, we confirmed that these EVs were well-tolerated as biocompatible agents, without a significant influence on food and water intake and noticeable pathological changes in tumor-bearing mice. Moreover, we observed activation of CD8^{+} lymphocytes expressing IFN-γ and GZMB and upregulation of macrophages, predominantly of the M1-like phenotype. In general, our study provides a promising immunotherapy strategy based on *Akk*-EVs, which might serve as an efficient and biocompatible tumor vaccine or tumor immunoadjuvant for PCa treatment.

Akk, an important commensal bacterium in the gut microbiota, is now widely investigated and considered a potential next–generation probiotic.[18] Recent studies have found that the reduction of *Akk* content in the gut is associated with various disease conditions. Supplementation with this bacterium can facilitate treatment of many metabolic and immune disorders, including obesity, inflammatory bowel disease, type 2 diabetes, and atherosclerosis.[34–36] Remarkably, *Akk* has also been reported to impact cancer immunotherapy. It was demonstrated that compared to those who showed no response to anti-PD-1-based immunotherapy, responding patients with non-small-cell lung cancer or renal cell carcinoma had relatively high levels of the bacterium *Akk*. Supplementation with *Akk* can restore the efficacy of PD-1 blockade therapy.[20] The mechanisms involved are being extensively studied. The protective effects of *Akk* have long been verified to be due to its ability to degrade mucin in the gut and its competitive adhesion in intestinal epithelial cells against pathogenic bacteria, thus facilitating functions of the gut epithelial barrier and body homeostasis.[19,37] Increasing studies have suggested that these beneficial effects can also be attributed to surface components or metabolites. A specific outer membrane protein derived from *Akk*, Amuc_1100, has been shown to improve the gut barrier and metabolism in obese and diabetic mice.[38] The role in host metabolic and immunological regulation may be explained by activation of Toll-like receptor (TLR) 2/4 and induction of cytokines, such as IL-10.[39] Interestingly, Amuc_1100 increased the proportion of CTLs in a mouse model of colitis-associated colorectal cancer to blunt tumorigenesis.[40] Similarly, the supplement of *Akk*-EVs regulates gut permeability by enhancing tight junction function and improves metabolic functions in high-fat diet-fed diabetic or obese mice.[22,41,42] Moreover, our recent work revealed that *Akk*-EVs recapitulate the effects of *Akk* on

promoting bone metabolism balance and protecting against osteoporosis.[23] In this study, we found that these EVs could elicit a protective effect via reducing the tumor burden in PCa mice.

The critical finding of our study is that *Akk*-EVs elicit significant immunoregulatory responses in the PCa microenvironment. The TME dynamically changes and plays a pivotal role during tumor initiation and progression.[43,44] The TME is composed of tumor cells, endothelial cells, stromal cells, immune cells, various signaling molecules, and extracellular matrix.[45] Macrophages, antigen-presenting cells, CD8^{+} T cells, CD4^{+} T cells, and other specific immune cells in the TME are of great importance in innate and adaptive tumor immunity.[45,46] Cytotoxic CD8^{+} T lymphocytes are the main effector cells in tumor immune responses.[47] Activated CD8^{+} T cells can infiltrate into tumor tissue and bind to tumor cell surface ligands via the T-cell receptor, leading to cell death through secretion of IFN-γ, granzyme, TNFα, or perforin.[48,49] Provenge (sipuleucel-T) and Prostvac, both PCa therapeutic vaccines, can present specific and immunogenic antigens and significantly stimulate CTL-related antitumor immune responses and have been approved or validated in more extensive clinical trials.[3,11,50] Macrophages are highly plastic and heterogeneous cells, and the M1 and M2 phenotypes represent the two distinct termini of the macrophage activation spectrum.[31,51] Generally, M1 macrophages have tumoricidal activity by producing inflammatory cytokines and activating the immune response.[52,53] On the other hand, local signals in the TME activate M2 macrophages to trigger tumor neovascularization, immunosuppression, and tumor extracellular matrix reorganization, contributing to PCa progression.[29,54] Recent studies have reported that an increase in polarized M2 macrophages may serve as a risk factor for PCa patients.[55] The analysis of PCa patients at different clinical stages revealed an apparent increase in the M2/M1 ratio, which was correlated with clinical values.[56] Similar to the PCa vaccine, in our study, *Akk*-EVs therapy was sufficient to activate CD8^{+} T lymphocytes and promote T cell effector function, as reflected by the observed upregulation of the number of cells expressing IFN-γ or GZMB both in vivo and in vitro. Interestingly, our data demonstrated that *Akk*-EVs treatment also led to recruitment and polarization of macrophages to an M1-like phenotype both in the TME and in vitro. In addition, CM from *Akk*-EVs-treated macrophages elicited potent inhibition on the proliferation and invasion of PCa cells. Therefore, our findings confirmed that activated CTLs and polarized macrophages partly convey the antitumor strength of *Akk*-EVs.

One limitation of our study is that we did not clarify the molecular mechanism by which *Akk*-EVs regulate these immune changes in the PCa TME. Delivery of various bioactive molecules is the key mechanism by which EVs serve as effective therapeutic vehicles in cancer.[57,58] EVs derived from Gram-negative bacteria, such as *Akk*, referred to as outer membrane vesicles, can transfer pathogen-associated molecular patterns and multiple antigens (such as lipopolysaccharides, peptidoglycans, and bacterial nucleic acids), which can be recognized by Toll-like receptors or Nod-like receptors in immune cells.[59,60] Thus, EVs can induce a series of potent inflammatory and immune responses.[27,61] A previous study reported that EVs derived from *E. coli* effectively induced long-term antitumor immune responses in colon tumor-bearing mice, and mechanistic studies revealed that this antitumor effect is dependent on IFN-γ production, which is similar to our findings.[62] Furthermore, their results suggest that trypsin-sensitive surface proteins in bacterial EVs may be the key factors involved in IFN-γ production. However, the contents incorporated in bacterial EVs may vary due to the differences in bacterial origin and modulate immune responses in different TMEs. Specific active components and pattern recognition receptors may also be involved in the *Akk*-EVs-mediated protective effects in PCa treatment. Nevertheless, it should be noted that we could not rule out an impact of *Akk*-EVs on other specific immune cell types, such as natural killer cells and dendritic cells, which are also involved in tumor immunity. Thus, further explorations are required to determine the underlying mechanisms.

Recent evidence has shown effective treatment options for castration-resistant PCa, such as novel chemotherapeutics, androgen receptor inhibitors, and poly ADP-ribose polymerase (PARP) inhibitors.[3,4] Numerous clinical trials are also currently evaluating the efficacy and safety of these combination strategies.[5,6] For instance, KEYNOTE-365 is carried out to assess the combination of pembrolizumab (immune checkpoint inhibitor) with docetaxel, Olaparib (PARP inhibitor), or other intervention in patients with metastatic castration-resistant PCa (NCT02861573). Future studies will be of great value to investigate whether *Akk*-EVs in well-designed combination with other agents may exhibit robust synergistic antitumor effects in PCa therapy.

It is also worth noting that bacteria-derived EVs often carry several immunogens, such as lipopolysaccharide, which can trigger systemic side effects.[63] Consistent with numerous studies showing the safety of bacterial EVs, our experiments also confirmed no notable toxic effects in immune-competent mice.[62,64,65] Further studies are needed to systematically observe and comprehensively evaluate the long-term effects and safety of *Akk*-EVs application for cancer therapy.

Conclusion

In summary, *Akk*-EVs provoked antitumor immunity against PCa, including activation of CTLs and polarization of macrophages into the tumor-killing M1-like type. Therefore, our study suggests a promising immunotherapy strategy based on *Akk*-EVs for PCa treatment.

Abbreviations

PCa, prostate cancer; EVs, extracellular vesicles; *Akk, Akkermansia muciniphila; Akk*-EVs, *Akkermansia muciniphila*-derived EVs; CTLs, cytotoxic T lymphocytes; Mφ, macrophages; GZMB, granzyme B; IFN-γ, interferon γ; TME, tumor microenvironment; PD-1, programmed cell death protein 1; TLR, toll-like receptor; CM, condition medium; OD, optical density; TEM, transmission electron microscopy; DLS, dynamic light scattering; CCK-8, cell counting kit-8; FBS, fetal bovine serum; PMA, phorbol 12-myristate 13-acetate; FMO, Fluorescence Minus One; DAPI, 4′,6-diamidino-2-phenylindole; PBS, phosphate buffer saline; PCR, polymerase chain reaction; CT, cycle threshold; GAPDH, glyceraldehyde-phosphate dehydrogenase; INOS, inducible nitric oxide synthase; SEM, standard error of mean.

Acknowledgments

Disclosure

The authors report no conflicts of interest in this work.

References

1. Siegel RL, Miller KD, Jemal A. Cancer statistics, 2020. *CA Cancer J Clin*. 2020;70(1):7–30. doi:10.3322/caac.21590
2. Culp MB, Soerjomataram I, Efstathiou JA, Bray F, Jemal A. Recent global patterns in prostate cancer incidence and mortality rates. *Eur Urol*. 2020;77(1):38–52. doi:10.1016/j.eururo.2019.08.005
3. Nuhn P, De Bono JS, Fizazi K, et al. Update on systemic prostate cancer therapies: management of metastatic castration-resistant prostate cancer in the era of precision oncology. *Eur Urol*. 2019;75 (1):88–99. doi:10.1016/j.eururo.2018.03.028
4. Ku SY, Gleave ME, Beltran H. Towards precision oncology in advanced prostate cancer. *Nat Rev Urol*. 2019;16(11):645–654. doi:10.1038/s41585-019-0237-8
5. Powers E, Karachaliou GS, Kao C, et al. Novel therapies are changing treatment paradigms in metastatic prostate cancer. *J Hematol Oncol*. 2020;13(1):144. doi:10.1186/s13045-020-00978-z
6. Cha HR, Lee JH, Ponnazhagan S. Revisiting immunotherapy: a focus on prostate cancer. *Cancer Res*. 2020;80(8):1615–1623. doi:10.1158/ 0008-5472.CAN-19-2948
7. Burugu S, Dancsok AR, Nielsen TO. Emerging targets in cancer immunotherapy. *Semin Cancer Biol*. 2018;52(Pt 2):39–52.
8. Palucka A, Coussens L. The basis of oncoimmunology. *Cell*. 2016;164(6):1233–1247. doi:10.1016/j.cell.2016.01.049
9. Fritz JM, Lenardo MJ. Development of immune checkpoint therapy for cancer. *J Exp Med*. 2019;216(6):1244–1254. doi:10.1084/ jem.20182395
10. Lee P, Gujar S. Potentiating prostate cancer immunotherapy with oncolytic viruses. *Nat Rev Urol*. 2018;15(4):235–250. doi:10.1038/ nrurol.2018.10
11. Kantoff PW, Higano CS, Shore ND, et al. Sipuleucel-T immunotherapy for castration-resistant prostate cancer. *N Engl J Med*. 2010;363 (5):411–422. doi:10.1056/NEJMoa1001294
12. Beer TM, Kwon ED, Drake CG, et al. Randomized, double-blind, Phase III trial of ipilimumab versus placebo in asymptomatic or minimally symptomatic patients with metastatic chemotherapy-naive castration-resistant prostate cancer. *J Clin Oncol*. 2017;35(1):40–47. doi:10.1200/JCO.2016.69.1584
13. Song W, Das M, Chen X. Nanotherapeutics for immuno-oncology: a crossroad for new paradigms. *Trends Cancer*. 2020;6(4):288–298. doi:10.1016/j.trecan.2020.01.011
14. Goldberg MS. Improving cancer immunotherapy through nanotechnology. *Nat Rev Cancer*. 2019;19(10):587–602. doi:10.1038/s41568-019-0186-9
15. Wiklander O, Brennan MA, Lotvall J, Breakefield XO, El AS. Advances in therapeutic applications of extracellular vesicles. *Sci Transl Med*. 2019;11(492):v8521. doi:10.1126/scitranslmed.aav8521
16. Xu Z, Zeng S, Gong Z, Yan Y. Exosome-based immunotherapy: a promising approach for cancer treatment. *Mol Cancer*. 2020;19 (1):160. doi:10.1186/s12943-020-01278-3
17. Qin M, Du G, Sun X. Biomimetic cell-derived nanocarriers for modulating immune responses. *Biomater Sci*. 2020;8(2):530–543. doi:10.1039/C9BM01444F

18. Zhai Q, Feng S, Arjan N, Chen W. A next generation probiotic, Akkermansia muciniphila. *Crit Rev Food Sci Nutr*. 2019;59 (19):3227–3236. doi:10.1080/10408398.2018.1517725

19. Zhang T, Li Q, Cheng L, Buch H, Zhang F. Akkermansia muciniphila is a promising probiotic. *Microb Biotechnol*. 2019;12(6):1109–1125. doi:10.1111/1751-7915.13410

20. Routy B, Le Chatelier E, Derosa L, et al. Gut microbiome influences efficacy of PD-1-based immunotherapy against epithelial tumors. *Science*. 2018;359(6371):91–97. doi:10.1126/science.aan3706

21. Everard A, Belzer C, Geurts L, et al. Cross-talk between Akkermansia muciniphila and intestinal epithelium controls diet-induced obesity. *Proc Natl Acad Sci U S A*. 2013;110 (22):9066–9071. doi:10.1073/pnas.1219451110

22. Chelakkot C, Choi Y, Kim DK, et al. Akkermansia muciniphila-derived extracellular vesicles influence gut permeability through the regulation of tight junctions. *Exp Mol Med*. 2018;50(2): e450. doi:10.1038/emm.2017.282

23. Liu JH, Chen CY, Liu ZZ, et al. Extracellular vesicles from child gut microbiota enter into bone to preserve bone mass and strength. *Adv Sci (Weinh)*. 2021.

24. Yin H, Chen CY, Liu YW, et al. Synechococcus elongatus PCC7942 secretes extracellular vesicles to accelerate cutaneous wound healing by promoting angiogenesis. *Theranostics*. 2019;9(9):2678–2693. doi:10.7150/thno.31884

25. Wang ZX, Chen CY, Wang Y, et al. Ångstrom-scale silver particles as a promising agent for low-toxicity broad-spectrum potent anticancer therapy. *Adv Funct Mater*. 2019;29(23):1808556. doi:10.1002/adfm.201808556

26. Luo ZW, Li FX, Liu YW, et al. Aptamer-functionalized exosomes from bone marrow stromal cells target bone to promote bone regeneration. *Nanoscale*. 2019;11(43):20884–20892. doi:10.1039/C9NR02791B

27. Li M, Zhou H, Yang C, et al. Bacterial outer membrane vesicles as a platform for biomedical applications: an update. *J Control Release*. 2020;323:253–268. doi:10.1016/j.jconrel.2020.04.031

28. Toyofuku M, Nomura N, Eberl L. Types and origins of bacterial membrane vesicles. *Nat Rev Microbiol*. 2019;17(1):13–24. doi:10.1038/s41579-018-0112-2

29. Lopez-Bujanda Z, Drake CG. Myeloid-derived cells in prostate cancer progression: phenotype and prospective therapies. *J Leukoc Biol*. 2017;102(2):393–406. doi:10.1189/jlb.5VMR1116-491RR

30. Hayashi T, Fujita K, Matsushita M, Nonomura N. Main inflammatory cells and potentials of anti-inflammatory agents in prostate cancer. *Cancers (Basel)*. 2019;11(8):1153. doi:10.3390/cancers11081153

31. Luo ZW, Liu PP, Wang ZX, Chen CY, Xie H. Macrophages in osteosarcoma immune microenvironment: implications for immunotherapy. *Front Oncol*. 2020;10:586580. doi:10.3389/fonc.2020.586580

32. Chavez-Galan L, Olleros ML, Vesin D, Garcia I. Much more than M1 and M2 macrophages, there are also CD169(+) and TCR(+) macrophages. *Front Immunol*. 2015;6:263. doi:10.3389/fimmu.2015.00263

33. Hu X, Rao S, Tan Y, et al. Fructose-coated Angstrom silver inhibits osteosarcoma growth and metastasis via promoting ROS-dependent apoptosis through the alteration of glucose metabolism by inhibiting PDK. *Theranostics*. 2020;10(17):7710–7729. doi:10.7150/thno.45858

34. Hanninen A, Toivonen R, Poysti S, et al. Akkermansia muciniphila induces gut microbiota remodelling and controls islet autoimmunity in NOD mice. *Gut*. 2018;67(8):1445–1453. doi:10.1136/gutjnl-2017-314508

35. Dao MC, Everard A, Aron-Wisnewsky J, et al. Akkermansia muciniphila and improved metabolic health during a dietary intervention in obesity: relationship with gut microbiome richness and ecology. *Gut*. 2016;65(3):426–436. doi:10.1136/gutjnl-2014-308778

36. Li J, Lin S, Vanhoutte PM, Woo CW, Xu A. Akkermansia muciniphila protects against atherosclerosis by preventing metabolic endotoxemia-induced inflammation in Apoe-/- mice. *Circulation*. 2016;133(24):2434–2446. doi:10.1161/CIRCULATIONAHA.115.019645

37. Cheng D, Xie MZ. A review of a potential and promising probiotic candidate-Akkermansia muciniphila. *J Appl Microbiol*. 2020. doi:10.1111/jam.14911

38. Plovier H, Everard A, Druart C, et al. A purified membrane protein from Akkermansia muciniphila or the pasteurized bacterium improves metabolism in obese and diabetic mice. *Nat Med*. 2017;23 (1):107–113. doi:10.1038/nm.4236

39. Ottman N, Reunanen J, Meijerink M, et al. Pili-like proteins of Akkermansia muciniphila modulate host immune responses and gut barrier function. *PLoS One*. 2017;12(3):e173004. doi:10.1371/journal.pone.0173004

40. Wang L, Tang L, Feng Y, et al. A purified membrane protein from Akkermansia muciniphila or the pasteurised bacterium blunts colitis associated tumourigenesis by modulation of CD8(+) T cells in mice. *Gut*. 2020;69(11):1988–1997. doi:10.1136/gutjnl-2019-320105

41. Ashrafian F, Shahriary A, Behrouzi A, et al. Akkermansia muciniphila-derived extracellular vesicles as a mucosal delivery vector for amelioration of obesity in mice. *Front Microbiol*. 2019;10:2155. doi:10.3389/fmicb.2019.02155

42. Lee H, Lee Y, Kim J, et al. Modulation of the gut microbiota by metformin improves metabolic profiles in aged obese mice. *Gut Microbes*. 2018;9(2):155–165. doi:10.1080/19490976.2017.1405209

43. Quail DF, Joyce JA. Microenvironmental regulation of tumor progression and metastasis. *Nat Med*. 2013;19(11):1423–1437. doi:10.1038/nm.3394

44. Binnewies M, Roberts EW, Kersten K, et al. Understanding the tumor immune microenvironment (TIME) for effective therapy. *Nat Med*. 2018;24(5):541–550. doi:10.1038/s41591-018-0014-x

45. Roma-Rodrigues C, Mendes R, Baptista PV, Fernandes AR. Targeting tumor microenvironment for cancer therapy. *Int J Mol Sci*. 2019;20(4):840. doi:10.3390/ijms20040840

46. Vitkin N, Nersesian S, Siemens DR, Koti M. The tumor immune contexture of prostate cancer. *Front Immunol*. 2019;10:603. doi:10.3389/fimmu.2019.00603

47. Jayaprakash P, Ai M, Liu A, et al. Targeted hypoxia reduction restores T cell infiltration and sensitizes prostate cancer to immunotherapy. *J Clin Invest*. 2018;128(11):5137–5149. doi:10.1172/JCI96268

48. Trapani JA, Smyth MJ. Functional significance of the perforin/granzyme cell death pathway. *Nat Rev Immunol*. 2002;2(10):735–747. doi:10.1038/nri911

49. Anker JF, Naseem AF, Mok H, Schaeffer AJ, Abdulkadir SA, Thumbikat P. Multi-faceted immunomodulatory and tissue-tropic clinical bacterial isolate potentiates prostate cancer immunotherapy. *Nat Commun*. 2018;9(1):1591. doi:10.1038/s41467-018-03900-x

50. Gulley JL, Borre M, Vogelzang NJ, et al. Phase III trial of PROSTVAC in asymptomatic or minimally symptomatic metastatic castration-resistant prostate cancer. *J Clin Oncol*. 2019;37 (13):1051–1061. doi:10.1200/JCO.18.02031

51. Lanciotti M, Masieri L, Raspollini MR, et al. The role of M1 and M2 macrophages in prostate cancer in relation to extracapsular tumor extension and biochemical recurrence after radical prostatectomy. *Biomed Res Int*. 2014;2014:486798. doi:10.1155/2014/486798

52. Travers M, Brown SM, Dunworth M, et al. DFMO and 5-Azacytidine Increase M1 macrophages in the tumor microenvironment of murine ovarian cancer. *Cancer Res*. 2019;79(13):3445–3454. doi:10.1158/0008-5472.CAN-18-4018

53. Chen D, Xie J, Fiskesund R, et al. Chloroquine modulates antitumor immune response by resetting tumor-associated macrophages toward M1 phenotype. *Nat Commun*. 2018;9(1):873. doi:10.1038/s41467-018-03225-9

54. Nenu I, Gafencu G, Popescu T, Kacso G. Lactate - A new frontier in the immunology and therapy of prostate cancer. *J Cancer Res Ther.* 2017;13(3):406–411. doi:10.4103/0973-1482.163692

55. Meng J, Liu Y, Guan S, et al. The establishment of immune infiltration based novel recurrence predicting nomogram in prostate cancer. *Cancer Med.* 2019;8(11):5202–5213. doi:10.1002/cam4.2433

56. Comito G, Giannoni E, Segura CP, et al. Cancer-associated fibroblasts and M2-polarized macrophages synergize during prostate carcinoma progression. *Oncogene.* 2014;33(19):2423–2431. doi:10.1038/onc.2013.191

57. Syn NL, Wang L, Chow EK, Lim CT, Goh BC. Exosomes in cancer nanomedicine and immunotherapy: prospects and challenges. *Trends Biotechnol.* 2017;35(7):665–676. doi:10.1016/j.tibtech.2017.03.004

58. Linxweiler J, Junker K. Extracellular vesicles in urological malignancies: an update. *Nat Rev Urol.* 2020;17(1):11–27. doi:10.1038/s41585-019-0261-8

59. Cao Z, Liu J. Bacteria and bacterial derivatives as drug carriers for cancer therapy. *J Control Release.* 2020;326:396–407. doi:10.1016/j.jconrel.2020.07.009

60. Wang S, Gao J, Wang Z. Outer membrane vesicles for vaccination and targeted drug delivery. *Wiley Interdiscip Rev Nanomed Nanobiotechnol.* 2019;11(2):e1523. doi:10.1002/wnan.1523

61. Cheng K, Kang Q, Zhao X. Biogenic nanoparticles as immunomodulator for tumor treatment. *Wiley Interdiscip Rev Nanomed Nanobiotechnol.* 2020;12(6):e1646. doi:10.1002/wnan.1646

62. Kim OY, Park HT, Dinh N, et al. Bacterial outer membrane vesicles suppress tumor by interferon-gamma-mediated antitumor response. *Nat Commun.* 2017;8(1):626. doi:10.1038/s41467-017-00729-8

63. Micoli F, MacLennan CA. Outer membrane vesicle vaccines. *Semin Immunol.* 2020;50:101433. doi:10.1016/j.smim.2020.101433

64. Li Y, Zhao R, Cheng K, et al. Bacterial outer membrane vesicles presenting programmed death 1 for improved cancer immunotherapy via immune activation and checkpoint inhibition. *ACS Nano.* 2020;14 (12):16698–16711. doi:10.1021/acsnano.0c03776

65. Qing S, Lyu C, Zhu L, et al. Biomineralized bacterial outer membrane vesicles potentiate safe and efficient tumor microenvironment reprogramming for anticancer therapy. *Adv Mater.* 2020;32(47): e2002085. doi:10.1002/adma.202002085